PROCEEDINGS OF SCIENCE

Recent results from Herschel on the filamentary structure of the cold interstellar medium

Philippe André[*†]

Laboratoire d'Astrophysique (AIM) de Paris-Saclay, CEA Saclay, 91191 Gif-sur-Yvette, France

E-mail: pandre@cea.fr

Recent developments in our observational understanding of the link between the structure of the cold interstellar medium and the star formation process are discussed. Extensive submillimeter studies of the nearest molecular clouds of our Galaxy with the *Herschel* Space Observatory have provided us with unprecedented images of the initial and boundary conditions of the star formation process. The *Herschel* images reveal an intricate network of filamentary structures in every interstellar cloud. The observed filaments share common properties – such as their central widths – but only the densest ones contain prestellar cores, the seeds of future stars. Overall, the *Herschel* submillimeter data favor a scenario in which interstellar filaments and prestellar cores represent two key steps in the star formation process: first large-scale supersonic MHD turbulence stirs up the gas, giving rise to a universal web-like structure in the ISM, then gravity takes over and controls the further fragmentation of filaments into prestellar cores and ultimately protostars. This scenario provides new insight into the inefficiency of star formation, the origin of the initial mass function, and the global rate of star formation in galaxies. Despite an apparent complexity, global star formation may be governed by relatively simple universal laws from filamentary clumps to galactic scales.

Cosmic Rays and the InterStellar Medium - CRISM 2014,
24-27 June 2014
Montpellier, France

[*]Speaker.

[†]This work has benefited from the support of the French National Research Agency (Grant no. ANR–11–BS56–0010 – STARFICH) and the European Research Council under the European Union's Seventh Framework Programme (ERC Grant Agreement no. 291294 – ORISTARS).

 http://pos.sissa.it/

PoS(CRISM2014)032

1. Introduction

Star formation is one of the most complex processes in astrophysics, involving a subtle interplay between gravity, turbulence, magnetic fields, feedback mechanisms, heating and cooling effects etc... Yet, despite this apparent complexity, the net products of the star formation process on global scales are relatively simple and robust. In particular, the distribution of stellar masses at birth or stellar initial mass function (IMF) is known to be quasi-universal (e.g. Kroupa 2002, Chabrier 2003, Elmegreen et al. 2008). Likewise, the star formation rate on both GMC and galaxy-wide scales is related to the mass of (dense molecular) gas available by rather well defined "star formation laws" (e.g. Kennicutt 1998, Lada et al. 2012). On the basis of recent results obtained with the *Herschel* Space Observatory on nearby interstellar clouds as part of the Gould Belt (André et al. 2010), HOBYS (Motte et al. 2010), and Hi-GAL (Molinari et al. 2010) surveys, the thesis advocated in this paper is that it may be possible to explain, at least partly, the IMF and the global rate of star formation in terms of the quasi-universal filamentary structure of the cold interstellar medium out of which stars form.

2. Universality of filamentary structures in the cold ISM

The high quality and dynamic range of the *Herschel* submillimeter dust continuum images are such that they provide key information on both dense cores on small (< 0.1 pc) scales *and* the structure of the parent clouds on large (> 1 pc) scales. In particular, one of the most spectacular early findings made with *Herschel* is the ubiquitous presence of long ($>$ pc scale) filamentary structures in the cold interstellar medium (ISM) and the apparently tight connection between the filaments and the formation process of dense cores (e.g. André et al. 2010; Men'shchikov et al. 2010). While interstellar clouds were already known to exhibit large-scale filamentary structures long before *Herschel* (e.g. Schneider & Elmegreen 1979; Hartmann 2002; Hatchell et al. 2005; Myers 2009), *Herschel* now demonstrates that these filaments are truly ubiquitous in the giant molecular clouds (GMCs) of our Galaxy (Molinari et al. 2010) and provides an unprecedented large-scale view of the role of filaments in the formation of prestellar cores (see § 3).

Remarkably, filaments are omnipresent even in diffuse, non-star-forming complexes such as the Polaris translucent cloud (cf. Fig. 1 – Miville-Deschênes et al. 2010; Ward-Thompson et al. 2010). Moreover, in any given cloud complex, the *Herschel* images reveal a whole network of filaments (see Figs. 1 & 2), making it possible to characterize their properties in a statistical manner. Detailed analysis of the radial column density profiles derived from *Herschel* data shows that the filaments are characterized by a very narrow distribution of central widths with a typical FWHM value of ~ 0.1 pc (Arzoumanian et al. 2011 – see Fig. 3a & 4). A plausible interpretation of this characteristic width of interstellar filaments is that it corresponds to the sonic scale below which interstellar turbulence becomes subsonic in diffuse, non-star-forming gas (cf. Padoan et al. 2001; Federrath et al. 2010).

3. The key role of filaments in the core formation process

The observed correspondence between the filaments and the spatial distribution of compact cores is also remarkable (see Fig. 5), suggesting that *dense cores form primarily along filaments*.

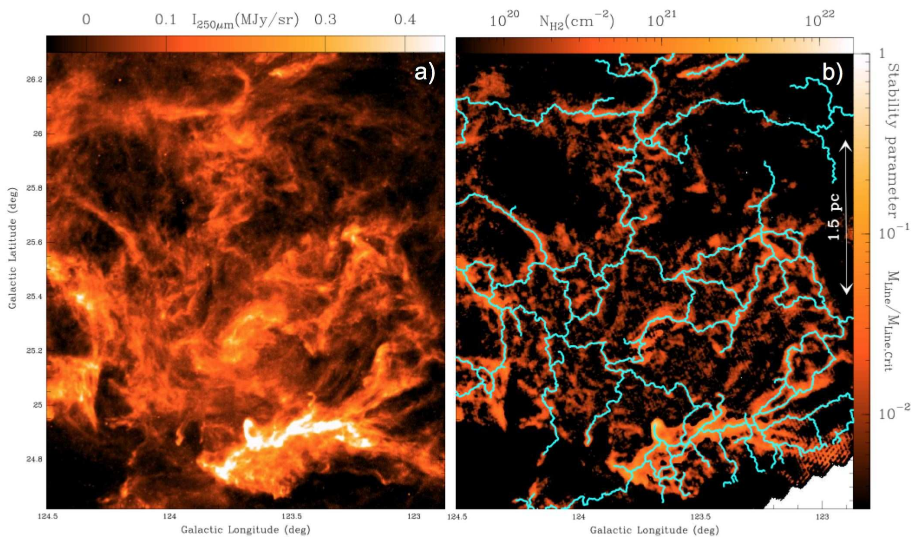

Figure 1: (a) *Herschel*/SPIRE 250 μm dust continuum map of a portion of the Polaris flare translucent cloud (e.g. Miville-Deschênes et al. 2010; Ward-Thompson et al. 2010). **(b)** Corresponding column density map derived from *Herschel* data (e.g. André et al. 2010). The contrast of the filaments has been enhanced using a curvelet transform (cf. Starck et al. 2003). The skeleton of the filament network identified with the DisPerSE algorithm (Sousbie 2011) is shown in light blue. A similar pattern is found with other algorithms such as *getfilaments* (Men'shchikov 2013). Given the typical width $\sim$ 0.1 pc of the filaments (Arzoumanian et al. 2011 – see Fig. 4 below), this column density map is equivalent to a *map of the mass per unit length along the filaments* (see color scale on the right).

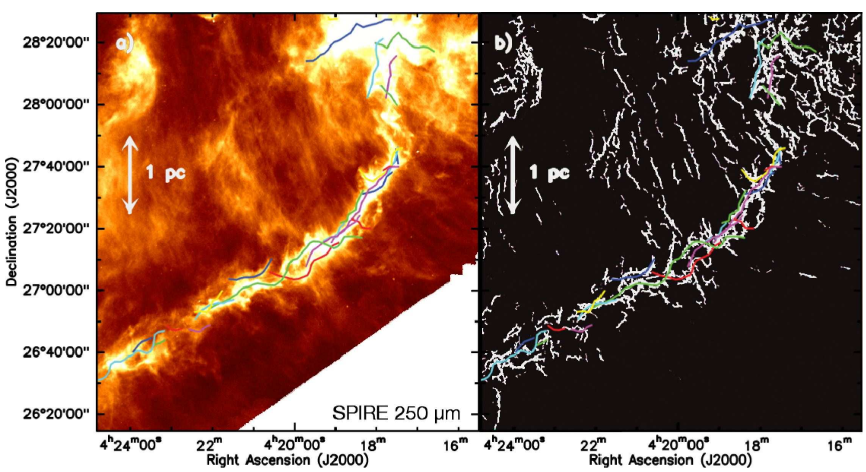

Figure 2: (a) *Herschel*/SPIRE 250 μm dust continuum image of the B211/B213/L1495 region in Taurus (Palmeirim et al. 2013). The colored curves display the velocity-coherent "fibers" identified within the B213/B211 filament by Hacar et al. (2013) using $C^{18}O$(1–0) observations. **(b)** Fine structure of the *Herschel*/SPIRE 250 μm dust continuum emission from the B211/B213 filament obtained by applying the multi-scale algorithm *getfilaments* (Men'shchikov 2013) to the 250 μm image shown in panel (a). Note the faint striations perpendicular to the main filament and the excellent correspondence between the small-scale structure of the dust continuum filament and the bundle of velocity-coherent fibers traced by Hacar et al. (2013) in $C^{18}O$ (same colored curves as in (a)).

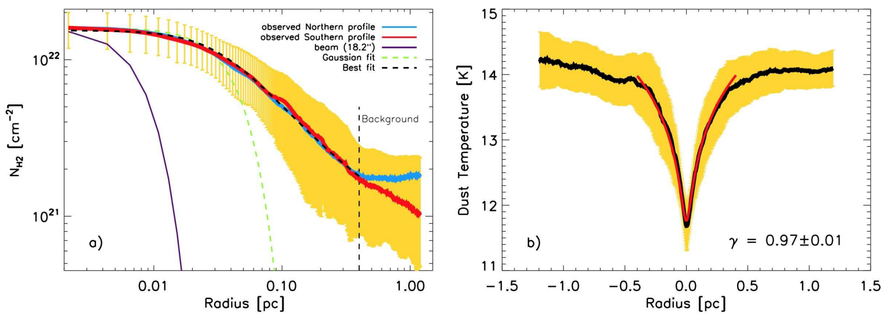

Figure 3: **(a)** Mean radial column density profile observed perpendicular to the B213/B211 filament in Taurus (Palmeirim et al. 2013), for both the Northern (blue curve) and the Southern part (red curve) of the filament. The yellow area shows the ($\pm 1\sigma$) dispersion of the distribution of radial profiles along the filament. The inner solid purple curve shows the effective 18" HPBW resolution (0.012 pc at 140 pc) of the *Herschel* column density map used to construct the profile. The dashed black curve shows the best-fit Plummer model (convolved with the 18" beam), which has a central diameter $2 \times R_{\rm flat} = 0.07 \pm 0.01$ pc and matches the data very well for $r \leq 0.4$ pc, **(b)** Mean dust temperature profile measured perpendicular to the B213/B211 filament in Taurus. The solid red curve shows the best polytropic model temperature profile obtained by assuming $T_{\rm gas} = T_{\rm dust}$ and that the filament has a density profile given by the Plummer model shown in the left panel and obeys a polytropic equation of state, $P \propto \rho^{\gamma}$ [and thus $T(r) \propto \rho(r)^{(\gamma-1)}$]. This best fit corresponds to a polytropic index γ=0.97±0.01 (see Palmeirim et al. 2013 for further details).

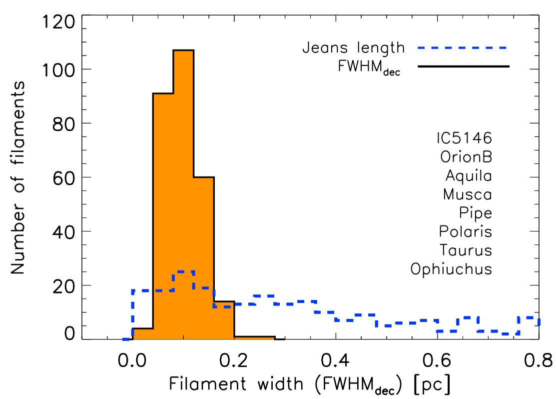

Figure 4: Histogram of deconvolved FWHM widths for a sample of 278 filaments in 8 nearby regions of the Gould Belt, all observed with *Herschel* (at resolutions ranging from ~ 0.01 pc to ~ 0.04 pc) and analyzed in the same way (Arzoumanian et al., in prep. – see Arzoumanian et al. 2011 for initial results on a subsample of 90 filaments in 3 clouds). The distribution of filament widths is narrow with a median value of 0.09 pc and a standard deviation of 0.04 pc (equal to the bin size). In contrast, the distribution of Jeans lengths corresponding to the central column densities of the filaments (blue dashed histogram) is much broader.

More precisely, the prestellar cores identified with *Herschel* are preferentially found within the *densest filaments* with masses per unit length exceeding $\sim 16 M_{\odot}$/pc and column densities exceeding $\sim 7 \times 10^{21}$ cm^{-2} (André et al. 2010 and Fig. 5a).

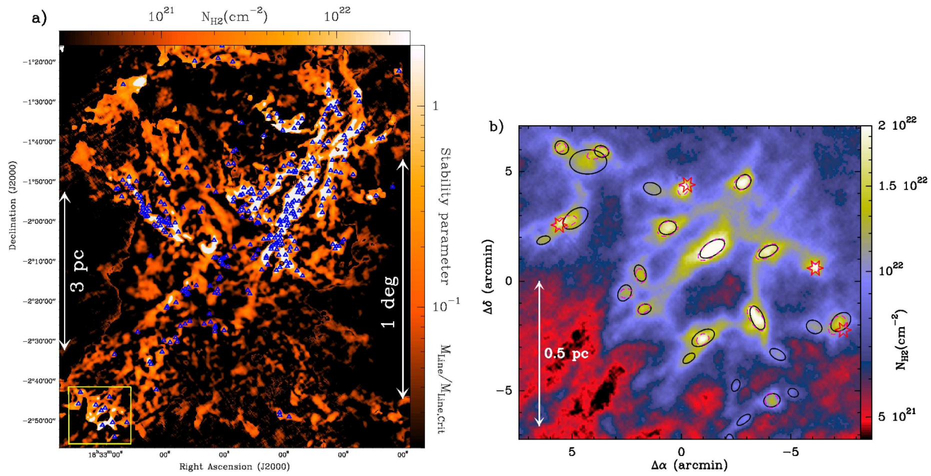

Figure 5: (a) Column density map of a subfield of the Aquila star-forming region derived from *Herschel* data (André et al. 2010). The contrast of the filaments has been enhanced using a curvelet transform (cf. Starck et al. 2003). Given the typical width ~ 0.1 pc of the filaments (Arzoumanian et al. 2011 – see Fig. 4), this map is equivalent to a *map of the mass per unit length along the filaments*. The areas where the filaments have a mass per unit length larger than half the critical value $2\,c_s^2/G$ (cf. Inutsuka and Miyama 1997) and are thus likely gravitationally unstable are highlighted in white. The bound prestellar cores identified by Könyves et al. (2010) are shown as small blue triangles. **(b)** Close-up column density map of the area shown as a yellow box on the left. The black ellipses mark the major and minor FWHM sizes of the prestellar cores found with the source extraction algorithm *getsources* (Men'shchikov et al. 2012); four protostellar cores are also shown by red stars. The dashed purple ellipses mark the FHWM sizes of the sources independently identified with the *csar* algorithm (J. Kirk et al. 2013). The effective resolution of the image is ~ 18" or ~ 0.02 pc at $d \sim 260$ pc.

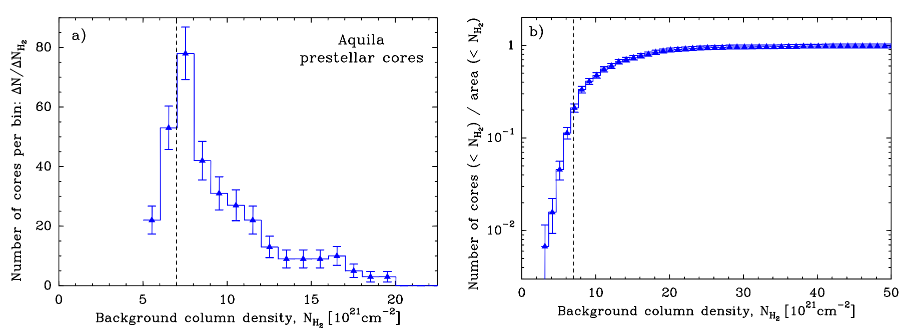

Figure 6: (a) Distribution of background column densities for the candidate prestellar cores identified with *Herschel* in the Aquila Rift complex (cf. Könyves et al. 2010 and in prep.). The vertical dashed line marks the column density or extinction threshold at $N_{\rm H_2}^{\rm back} \sim 7 \times 10^{21}$ cm^{-2} or $A_V^{\rm back} \sim 7$ (also corresponding to $\Sigma_{\rm gas}^{\rm back} \sim 150\ M_\odot\,{\rm pc}^{-2}$). **(b)** Normalized probability of finding a *Herschel* prestellar core below a given background column density in Aquila as a function of background column density (cf. from Könyves et al. in prep.). Note that this probability increases by more than one order of magnitude between $N_{\rm H_2}^{\rm back} \sim 4 \times 10^{21}$ cm^{-2} and $N_{\rm H_2}^{\rm back} \sim 10^{22}$ cm^{-2}. The vertical dashed line marks the same column density "threshold" at $A_V^{\rm back} \sim 7$ as in the left panel.

3.1 A column density threshold for prestellar core formation

In the Aquila region, for instance, the distribution of background cloud column densities for the prestellar cores (Fig. 6a) shows a steep rise above $N_{\rm H_2}^{\rm back} \sim 5 \times 10^{21}$ cm^{-2} and is such that $\sim 90\%$ of the candidate bound cores are found above a background column density $N_{\rm H_2}^{\rm back} \sim 7 \times 10^{21}$ cm^{-2}, corresponding to a background visual extinction $A_V^{\rm back} \sim 7$ (André et al. 2014; Könyves et al., in prep.). The *Herschel* observations of the Aquila Rift complex therefore strongly support the existence of a column density or visual extinction threshold for the formation of prestellar cores at $A_V^{\rm back} \sim 5$–10, which had been suggested based on earlier ground-based studies of, e.g., Taurus and Ophiuchus (cf. Onishi et al. 1998; Johnstone et al. 2004; Goldsmith et al. 2008). In the Polaris flare, the *Herschel* results are also consistent with such an extinction threshold since the observed background column densities are all below $A_V^{\rm back} \sim 8$ and there are no examples of bound prestellar cores in this cloud (André et al. 2010; Ward-Thompson et al. 2010).

We stress that two effects make this column density threshold very significant. First, the typical distribution of mass in star-forming clouds is such that there is much more low-density gas than high-density gas (in Aquila, for instance, $\sim 85\%$ of the cloud mass is below $A_V = 7$ and only $\sim 15\%$ of the mass lies at higher column densities). Second, the completeness of our *Herschel* census for prestellar cores increases in lower column density areas, due to a lower level of "cirrus noise" fluctuations (cf. Gautier et al. 1992). As a consequence, if prestellar cores were randomly distributed throughout the cloud independently of the local background (column) density, we would be much more likely to observe cores in lower column density areas. This is clearly not the case. Figure 6b shows the estimated probability of finding a *Herschel* prestellar core as a function of background column density, obtained by normalizing the number of *Herschel* prestellar cores identified below a given background column density by the total surface area imaged with *Herschel* below the same cloud column density in Aquila. It can be seen that this probability function resembles a smooth step function centered around $A_V^{\rm back} \sim 7$.

3.2 Interpretation of the star formation threshold

The *Herschel* results provide an *explanation* of the core/star formation threshold in terms of the filamentary structure of molecular clouds. Given the characteristic width ~ 0.1 pc measured for the filaments (Arzoumanian et al. 2011 – cf. Figs. 3a & 4), the threshold at $A_V^{\rm back} \sim 8$ or $\Sigma_{\rm gas}^{\rm back} \sim 150\, M_\odot\,{\rm pc}^{-2}$ corresponds to within a factor of $<< 2$ to the critical mass per unit length $M_{\rm line,crit} = 2c_s^2/G \sim 16 M_\odot$/pc required for the hydrostatic equilibrium of isothermal filaments (cf. Ostriker 1964), where $c_s \sim 0.2$ km/s is the isothermal sound speed for a typical gas temperature $T \sim 10$ K. Thus, the core formation threshold approximately corresponds to the *threshold above which interstellar filaments are gravitationally unstable* to both radial contraction and fragmentation along their lengths (cf. Inutsuka & Miyama 1992, 1997). Prestellar cores are only observed above this threshold because they form out of a filamentary background and only the supercritical, gravitationally unstable filaments with $M_{\rm line} > M_{\rm line,crit}$ are able to fragment into bound cores (cf. André et al. 2010 and Fig. 5a).

4. Origin of the characteristic width of interstellar filaments and role of accretion

The fact that the same ~ 0.1 pc width is measured for low-density, subcritical filaments and high-density, supercritical filaments suggests that this characteristic scale is set by the physical process(es) producing the filamentary structure in the first place. Furthermore, at least in the case of diffuse, gravitationally unbound clouds such as Polaris (Fig. 1), gravity is unlikely to be involved. Large-scale compression flows (turbulent or not) and the dissipation of the corresponding energy provide a potential mechanism. In the picture proposed by Padoan et al. (2001), for instance, the dissipation of turbulence occurs in shocks, and interstellar filaments correspond to dense, post-shock stagnation gas associated with compressed regions between interacting supersonic flows. One merit of this picture is that it can account qualitatively for the ~ 0.1 pc width. The typical thickness of shock-compressed structures resulting from supersonic turbulence in the ISM is indeed expected to be roughly the sonic scale of the turbulence, i.e., ~ 0.1 pc in diffuse interstellar gas (cf. Larson 1981; Federrath et al. 2010, and discussion in Arzoumanian et al. 2011). Direct evidence of the role of large-scale compressive flows has been found with *Herschel* in the Pipe Nebula in the form of filaments with asymmetric column density profiles which most likely result from compression by the winds of the nearby Sco OB2 association (Peretto et al. 2012).

A more complete picture, proposed by Hennebelle (2013), is that filaments result from a combination of turbulent compression and shear (see Hily-Blant & Falgarone 2009 for an observed example of a diffuse CO filament in Polaris corresponding to a region of intense velocity shear). Interestingly, the filament width is comparable to the cutoff wavelength $\lambda_A \sim 0.1\,\mathrm{pc} \times (\frac{\mathrm{B}}{10\ \mu\mathrm{G}}) \times (\frac{\mathrm{n_{H_2}}}{10^3\ \mathrm{cm^{-3}}})^{-1}$ below which MHD waves cannot propagate in the primarily neutral gas of molecular clouds (cf. Mouschovias 1991), if the typical magnetic field strength is $B \sim 10\,\mu$G in the low-density envelopes of molecular clouds (Crutcher 2012). Hence the tentative suggestion that the filament width may be set by the dissipation mechanism of MHD waves due to ion-neutral friction (Hennebelle 2013). Alternatively, the characteristic width may also be understood if interstellar filaments are formed as quasi-equilibrium structures in pressure balance with a typical ambient ISM pressure $P_{\rm ext}/k_{\rm B} \sim 2-5\times10^4\,\mathrm{K\,cm^{-3}}$ (Fischera and Martin 2012; Inutsuka et al., in prep.). Clearly, more work is needed to fully clarify the origin of the width of subcritical filaments.

That star-forming, supercritical filaments also maintain roughly constant inner widths ~ 0.1 pc while evolving (Arzoumanian et al. 2011 – see Figs. 3a & 4) is more surprising at first sight. Indeed, supercritical filaments are unstable to radial collapse and are thus expected to undergo rapid radial contraction with time (e.g. Inutsuka & Miyama 1997). The most likely solution to this paradox is that supercritical filaments are *accreting* additional background material while contracting. The increase in velocity dispersion with central column density observed for supercritical filaments (Arzoumanian et al. 2013) is indeed suggestive of an increase in (virial) mass per unit length with time.

More direct observational evidence of this accretion process for supercritical filaments exists in several cases in the form of low-density striations or sub-filaments seen perpendicular to the main filaments and apparently feeding them from the side (see Fig. 7). This process supplies gravitational energy to supercritical filaments which is then converted into turbulent kinetic energy (cf. Klessen & Hennebelle 2010) and may explain the observed increase in velocity dispersion with column density ($\sigma_{\rm tot} \propto {\Sigma_0}^{0.5}$ – Arzoumanian et al. 2013). Indeed, the fine substructure and velocity-coherent "fibers" observed within *Herschel* supercritical filaments (cf. Fig. 2 and Hacar et al. 2013) may possibly be the manifestation of such accretion-driven "turbulence". The central diameter of

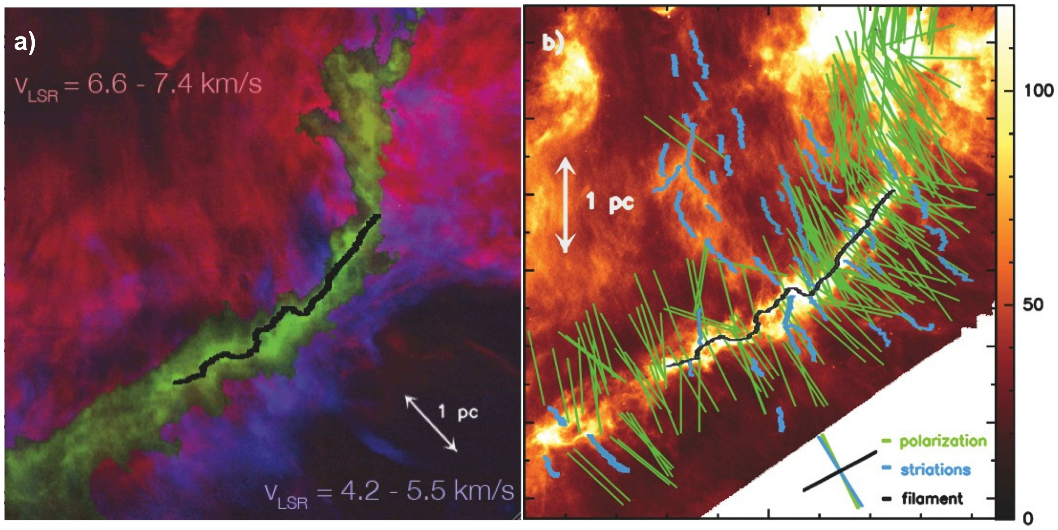

Figure 7: **(a)** Red-shifted and blue-shifted ^{12}CO(1–0) emission observed on either side of the B211/B213 filament in Taurus (Goldsmith et al. 2008), consistent with gravitational accretion of low-density background cloud material into the central filament (cf. Palmeirim et al. 2013). **(b)** Optical and infrared polarization vectors (green segments), tracing the plane-of-sky direction of the magnetic field, overlaid on the *Herschel*/SPIRE 250 μm image of the B211/B213 region. The blue segments mark low-density striations visible in the *Herschel* submillimeter dust continuum data (see also Fig. 2a) and suggestive of accretion flows along field lines into the B211/B213 filament. (From Palmeirim et al. 2013).

accreting filaments is expected to be of order the effective Jeans length $D_{\rm J,eff} \sim 2\,\sigma_{\rm tot}^2/G\Sigma_0$, which Arzoumanian et al. (2013) have shown to remain close to ~ 0.1 pc. Hence, through accretion of parent cloud material, supercritical filaments may keep roughly constant inner widths and remain in rough virial balance while contracting (see Heitsch 2013; Hennebelle & André 2013). This process may effectively prevent the global (radial) collapse of supercritical filaments and thus favor their fragmentation into cores (e.g. Larson 2005), in agreement with the *Herschel* results (see Fig. 5).

5. Conclusions: Toward a universal scenario for core and star formation?

The results obtained with *Herschel* on nearby clouds and summarized in the previous sections provide key insight into the first phases of the star formation process. They emphasize the role of filaments and support a scenario according to which the formation of prestellar cores occurs in two main steps (see, e.g., André et al. 2014). First, the dissipation of kinetic energy in large-scale MHD flows (turbulent or not) appears to generate ~ 0.1 pc-wide filaments in the cold neutral ISM. Second, the densest filaments fragment into prestellar cores by gravitational instability above the critical mass per unit length $M_{\rm line,crit} \approx 16\,M_\odot\,{\rm pc}^{-1}$, equivalent to a critical (column) density threshold $\Sigma_{\rm gas}^{\rm crit} \sim 160\,M_\odot\,{\rm pc}^{-2}$ ($A_V^{\rm crit} \sim 8$) or $n_{\rm H_2}^{\rm crit} \sim 2\times10^4\,{\rm cm}^{-3}$.

In contrast to the standard gravo-turbulent fragmentation picture (e.g., MacLow & Klessen 2004), in which filaments are present but play no fundamental role, this scenario relies heavily on the unique properties of filamentary geometry, such as the existence of a critical mass per unit length for nearly isothermal filaments.

That the formation of filaments in the diffuse ISM represents the first step toward core and star formation is suggested by the filaments *already* being pervasive in a gravitationally unbound, non-star-forming cloud such as Polaris (cf. Fig. 1; Hily-Blant and Falgarone 2007; Men'shchikov et al. 2010; Miville-Deschênes et al. 2010). Hence, many interstellar filaments are not produced by large-scale gravity and their formation must precede star formation.

The second step appears to be the gravitational fragmentation of the densest filaments with supercritical masses per unit length ($M_{\rm line} \geq M_{\rm line,crit}$) into prestellar cores (cf. André et al. 2010). In active star-forming regions such as the Aquila complex, most of the prestellar cores identified with *Herschel* are indeed concentrated within supercritical filaments (cf. Fig. 5a). In contrast, in non-star-forming clouds such as Polaris, all of the filaments have subcritical masses per unit length and very few (if any) prestellar cores and no protostars are observed (cf. Fig. 1).

The present scenario may explain the peak for the prestellar CMF and the base of the stellar IMF (see André et al. 2014). It partly accounts for the general inefficiency of the star formation process since, even in active star-forming complexes such as Aquila (Fig. 5), only a small fraction of the total gas mass ($\sim$ 15% in the case of Aquila) is above of the column density threshold, and only a small fraction $f_{\rm pre} \sim 15\%$ of the dense gas above the threshold is in the form of prestellar cores (Könyves et al., in prep.). Therefore, the vast majority of the gas in a GMC ($\sim$ 98% in the case of Aquila) does not participate in star formation at any given time (see also Heiderman et al. 2010). Furthermore, the fact that essentially the same "star formation law" is observed above the column density threshold in both Galactic clouds and external galaxies (Lada et al. 2012) suggests the star formation scenario sketched above may well apply to the ISM of other galaxies.

References

[1] André, Ph., Men'shchikov, A., Bontemps, S. et al. 2010, A&A, 518, L102

[2] André, Ph., Di Francesco, J., Ward-Thompson, D., Inutsuka, S., Pudritz, R., & Pineda, J. 2014, in Protostars and Planets VI, Eds. H. Beuther et al., in press (astro-ph/1312.6232)

[3] Arzoumanian, D., André, Ph., Didelon, P. et al. 2011, A&A, 529, L6

[4] Arzoumanian, D., André, Ph., Peretto, N., & Könyves, V. 2013, A&A, 553, A119

[5] Chabrier, G. 2003, PASP, 115, 763

[6] Crutcher, R. M. 2012, ARA&A, 50, 29

[7] Elmegreen, B.G., Klessen, R.S., & Wilson, C.D. 2008, ApJ, 681, 365

[8] Federrath, C., Roman-Duval, J., Klessen, R.S. et al. 2010, A&A, 512, A81

[9] Fischera, J., & Martin, P.G. 2012, A&A, 542, A77

[10] Gao, Y., & Solomon, P. 2004, ApJ, 606, 271

[11] Gautier, T.N., Boulanger, F., Pérault, M., Puget, J.L. 1992, AJ, 103, 1313

[12] Goldsmith, P.F., Heyer, M., Narayanan, G. et al. 2008, ApJ, 680, 428

[13] Hacar, A., Tafalla, M., Kauffmann, J., & Kovacs, A. 2013, A&A, 554, A55

[14] Hartmann, L. 2002, ApJ, 578, 914

[15] Hatchell, J., Richer, J. S., Fuller, G. A. et al. 2005, A&A, 440, 151

[16] Heiderman, A., Evans, N.J., Allen, L.E. et al. 2010, ApJ, 723, 1019

[17] Heitsch, F. 2013, ApJ, 769, 115

[18] Hennebelle, P. 2013, A&A, 556, A153

[19] Hennebelle, P., & André, Ph. 2013, A&A, 560, A68

[20] Hily-Blant, P., & Falgarone, E. 2007, A&A, 469, 173

[21] Hily-Blant, P., & Falgarone, E. 2009, A&A, 500, L29

[22] Inutsuka, S-I, & Miyama, S.M. 1992, ApJ, 388, 392

[23] Inutsuka, S-I, & Miyama, S.M. 1997, ApJ, 480, 681

[24] Johnstone, D., Di Francesco, J., & Kirk, H. 2004, ApJ, 611, L45

[25] Kennicutt, R. 1998, ApJ, 498, 541

[26] Kirk, J.M., Ward-Thompson, D., Palmeirim, P. et al. 2013, MNRAS, 432, 1424

[27] Klessen, R. S., & Hennebelle, P. 2010, A&A, 520, A17

[28] Könyves, V., André, Ph., Men'shchikov, A. et al. 2010, A&A, 518, L106

[29] Kroupa, P. 2002, Science, 295, 82

[30] Lada, C.J., Forbrich, J., Lombardi, M, & Alves, J. F. 2012, ApJ, 745, 190

[31] Larson, R.B. 1981, MNRAS, 194, 809

[32] Larson, R. B. 2005, MNRAS, 359, 211

[33] MacLow, M.-M., & Klessen, R.S. 2004, RvMP, 76, 125

[34] Men'shchikov, A., André, Ph., Didelon, P. et al. 2010, A&A, 518, L103

[35] Men'shchikov, A., André, Ph., Didelon, P., Motte, F. et al. 2012, A&A, 542, A81

[36] Men'shchikov, A. 2013, A&A, 560, A63

[37] Miville-Deschênes, M.-A., Martin, P.G., Abergel, A. et al. 2010, A&A, 518, L104

[38] Molinari, S., Swinyard, B., Bally, J. et al. 2010, A&A, 518, L100

[39] Motte, F., Zavagno, A., Bontemps, S. et al. 2010, A&A, 518, L77

[40] Mouschovias, T. Ch. 1991, ApJ, 373, 169

[41] Myers, P.C. 2009, ApJ, 700, 1609

[42] Onishi, T., Mizuno, A., Kawamura, A. et al. 1998, ApJ, 502, 296

[43] Ostriker, J. 1964, ApJ, 140, 1056

[44] Padoan, P., Juvela, M., Goodman, A.A., & Nordlund, A. 2001, ApJ, 553, 227

[45] Palmeirim, P., André, Ph., Kirk, J. et al. 2013, A&A, 550, A38

[46] Peretto, N., André, Ph., Könyves, V. et al. 2012, A&A, 541, A63

[47] Schneider, S. & Elmegreen, B.G. 1979, ApJS, 41, 87

[48] Sousbie, T., 2011, MNRAS, 414, 350

[49] Starck, J. L., Donoho, D. L., Candès, E. J. 2003, A&A, 398, 785

[50] Ward-Thompson, D., Kirk, J.M., André, P. et al. 2010, A&A, 518, L92